Pis'ma v ZhETF, vol. 94, iss. 1, pp. 58 – 62 © 2011 July 10

Metallic glass electronic structure peculiarities revealed by UHV STM/STS

A. I. Oreshkin[+1)], *N. S. Maslova*[+], *V. N. Mantsevich*[+], *S. I. Oreshkin*[+*], *S. V. Savinov*[+], *V. I. Panov*[+], *D. V. Louzguine-Luzgin*[△]

[+]*Department of Physics, Moscow State University, 119992 Moscow, Russia*

[*] *Sternberg Astronomical Institute, Moscow State University, 119992, Moscow, Russia*

[△] *WPI-AIMR, Tohoku University 2-1-1 Katahira, Aoba-ku, 980-8577 Sendai, Japan*

Submitted 10 May 2011

We present the results of Ultra high vacuum scanning tunneling microscopy/spectroscopy investigation of metallic glass surface. The topography and electronic structure of $Ni_{63.5}Nb_{36.5}$ have been studied. A great number of clusters with size about 5–10 nm have been found on constant current STM images. The tunneling spectra of normalized tunneling conductivity revealed the energy pseudogap in the vicinity of Fermi energy. For energy values above 0.1 eV the normalized tunneling conductivity changes linearly with increasing of tunneling bias. The obtained results can be understood within suggested theoretical model based on the interplay of elastic electron scattering on random defects and weak intra-cluster Coulomb interaction. The effects of the finite edges of electron spectrum of each cluster have to be taken into account to explain the experimental data. The tunneling conductivity behavior and peculiarities in current images of individual clusters can be also qualitatively analysed in the framework of suggested model.

1. Introduction. Amorphous metallic glasses have been classified in a separate class of materials starting from classic rapid-quenching experiments on AuSi alloys performed by Duwez and colleagues [1]. Later a new class of metallic glasses called bulk metallic glasses with high glass-forming ability has been invented [2, 3]. The physical and chemical properties of metallic alloys in amorphous state are significantly different from the properties of metallic alloys in crystalline state. The strength and hardness values of amorphous alloys are higher than crystals have, while elastic modulus is slightly lower than in crystalline state. An elastic modulus difference can be caused by more loosely packed structure of metallic glasses due to lower number of the nearest neighbors in atomic structure. The "disordered" local structure of metallic glasses is responsible for their strength, hardness and formability. It has been also suggested that the main reason for high corrosion resistance is the absence of specific crystallographically "ordered" defects, which are typical for crystal structure. Such a unique combination of alloys properties is very important for creation of new materials with predefined parameters. Thus intensive experimental and theoretical investigations of such structures on nanoscale are of great importance at present. The microtopography of the nanometer-scale defects in metallic glasses has been studied recently by means of transmission electron microscopy [4]. Scanning tunneling microscopy (STM) [6, 7] was also applied [5] to get movies of the surface of metallic glasses with time resolution as fast as 1 minute and extending up to 1000 minutes. It was shown that rearrangements of surface clusters occur almost exclusively by two-state hopping. The majority of investigations dedicated to study metallic glasses were oriented to get information about microtopography of surface. Transmission electron microscope and difraction methods have been applied for these purposes mostly [8]. The spectroscopic information was obtained from photoemission experiments [9]. The structure of $Ni_{62}Nb_{38}$ metallic glass have been also investigated by neutron inelastic scattering [10]. The employment of scanning tunneling microscopy/spectroscopy (STM/STS) in the frame of this work allows to study topography and performs spectroscopic investigation of the surfaces of metallic glasses on the nanometer size area. Thefore the structural investigations combined with local electronic structure analysis using STM/STS are vital and attractive to analyze the microscopic origin of metallic glasses unusual properties.

2. Experimental procedure. We performed STM/STS study of bulk metallic glasses surface topography and electronic properties. Metallic glass $Ni_{63.5}Nb_{36.5}$ (bulk samples, prepared in 1 mm diameter rod shape [11]) were prepared at Tohoku University in Prof. Louzguine group. Ni-based metallic glass was chosen owing to its higher thermal stability versus

[1)]e-mail: oreshkin@spmlab.phys.msu.su

crystallization compared to Cu- and Zr-based glasses [12]. Then they were cut along the length to fit the STM-sample holder. The surface suitable for STM/STS study was obtained by grinding prosess with futher treatment of the surface using polishing slurry with particle sizes of 5, 1, and 0.05 μm to get flat and mirror like surface. The quality of prepared surface was controlled by optical microscope. Before installing samples in STM-holder they were ultrasonically cleaned in acetone and distilled water. Samples were degassed at 400 °C during 24 hours and processed with argon-ion-sputtering (1.5 kV, 30 μA, 60 min) at $9.0 \cdot 10^{-6}$ torr argon pressure. At the final stage of surface preparation the samples were heated again at 400 °C (which is 257 °C below its crystallization temperature of 657 °C [11]) during 12 hours at 10^{-10} torr pressure range. All experiments were performed using commercial UHV Omicron system with base pressure $1 \cdot 10^{-10}$ torr at room temperature. In our experiments we used tungsten tips obtained by electrochemical etching. To remove the oxide layer from the STM-tip apex, they were annealed at 1200 °C at ultra high vacuum conditions ($1.0 \cdot 10^{-10}$ torr). All the STM-images presented here are the constant current and the current imaging tunneling spectroscopy images (CITS) with bias voltage applied to the sample, while STM tip is virtually grounded. The constant current images are 400 × 400 points in size, while the CITS-images are 80 × 80 points. The $I(V)$ spectrum was taken at each fifth point of each fifth line of the scanning frame.

3. Theoretical model and main results. Typical constant current image of $Ni_{63.5}Nb_{36.5}$ surface is presented in Fig. 1. The STM-imaging showed that surface consists of clusters with typical size of about 5–10 nm. We were not able to observe any ordered structure in our STM images. We suppose that the sample surface can be treated as a disordered structure formed by set of random clusters. The size of each cluster d as well as its spectrum ε_p are random values. The spectrum boundaries of i-th cluster are A_i-lower one and W_i-upper one. The positions of the spectrum boundaries relative to the Fermi level $E_{\rm F}$ are also random. The observed behavior of tunneling conductivity spectrum $\sigma_T(eV)$, averaged over a large number of clusters, demonstrates the energy pseudogap in the vicinity of $E_{\rm F}$. Moreover one can observe linear part in dependence of tunneling conductivity on applied bias ($\sigma_T(eV) \sim eV$ for $eV \gtrsim 0.1$). To explain such behavior of $\sigma_T(eV)$ we suggest a simple model taking into account the elastic scattering of electrons on the impurities inside each cluster and on the random deffects on the cluster boundaries in the presence of intra-cluster Coulomb interaction of scattering

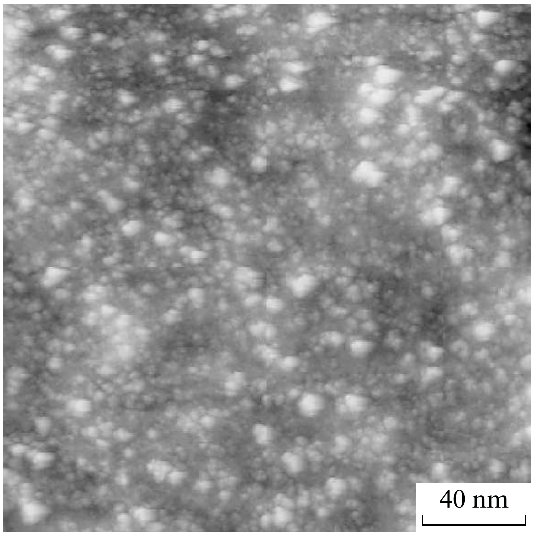

Fig. 1. Typical STM-constant current image of $Ni_{63.5}Nb_{36.5}$ surface; $20 \times 20\,\mathrm{nm}^2$; $V = -1.5\,\mathrm{V}$; $I = 57\,\mathrm{pA}$

electrons. Similar model has been used to obtain weak localization (WL) corrections to the electron density of states in weak localization regime [13–16]. The i-th cluster can be described by hamiltonian:

$$\hat{H}^i_{cl} = \sum_{p,\sigma} \varepsilon^i_p c^{+i}_{p\sigma} c^i_{p\sigma} + \sum_{p,p'} U_{pp'} c^{+i}_{p\sigma} c^i_{p'\sigma} + \\ + \sum_{p,p',g} V_g c^{+i}_p c^{+i}_{p'} c^i_{p-g} c^i_{p'+g} + \text{h.c.} \qquad (1)$$

The first term of Hamiltonian $\hat{H}^i_{cl}$ describes the free electrons with spin σ and momentum p within each cluster, the second one corresponds to the electron scattering inside the i-th cluster on random defects potential and the third term decribes the Coulomb interaction inside i-th cluster. Here $V_g = e^2/g^2$ – bare Coulomb interaction in Fourier representation, $c^i_{p\sigma}/c^{+i}_{p\sigma}$ – operators of annihilation/creation of cluster's electrons with spin σ. The fourier transform of random potential responsible for the electron scattering inside the i-th cluster is described by $U_{pp'}$. The correlation function of random potential is

$$\langle U_{pp'} \cdot U_{pp''} \rangle = \overline{U^2} \delta(p'' - p').$$

In WL-regime the interplay of $U_{pp'}$ and V_g results in changes of cluster density of states: $\nu(\varepsilon) = \nu_0 + \delta\nu(\varepsilon)$, ν_0 is unperturbed density of states (DOS), $\delta\nu(\varepsilon)$ – changes caused by the interaction. We also consider that the inter-cluster interaction is weak compared with intra-cluster one and leads to small corrections to $\nu(\varepsilon)$. The changes of local density of states (LDOS) caused by tunneling current and non-equilibrium effects are not

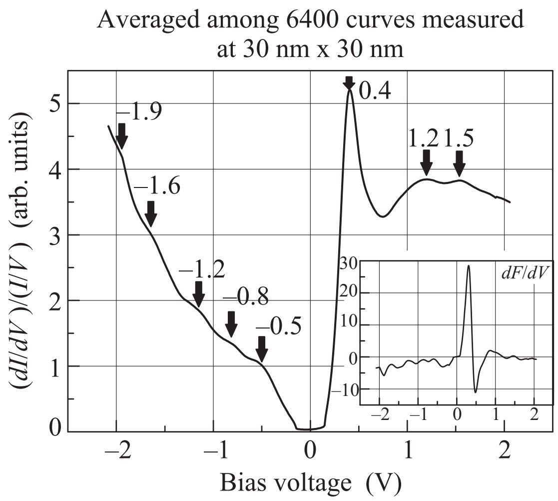

Fig. 2. DOS of $Ni_{63.5}Nb_{36.5}$ surface, obtained by averaging 6400 curves, measured at every 5-th point of $30 \times 30\,\mathrm{nm}^2$ constant current image. The first derivative of depicted curve is shown in the insert

taken into account in this approach. Let's determine the main scales of the model: E_{F}, p_{F}, V_{F} – Fermi energy, momentum and velocity correspondingly. In the following discussion we are using CGS-system of units; $\hbar\tau^{-1} = \overline{U}^2\nu_0 = \gamma$ – elastic scattering rate, τ – elastic scattering time, τ_φ – characteristic time of inelastic scattering (dephasing time); $D \sim V_{\mathrm{F}}^2\tau$ – diffusion coefficient due to elastic electron scattering; $l = V_{\mathrm{F}}\tau$ – mean electrons scattering length, d – the cluster size, $\lambda = 4\pi e^2\nu_0$ – Thomas–Fermi screening length of Colomb interaction. In WL-regime

$$\frac{p_{\mathrm{F}} l}{\hbar} \gg 1; \frac{\omega\tau}{\hbar} \ll 1,$$

where ω – the electron energy changes caused by inelastic Coulomb interaction.Taking into account the renormalization of Coulomb interaction by elastic electron scattering on random impurity potential and finite values of electron energy spectrum boundaries for i-th cluster one can obtain the changes of electron DOS similar to [17–19]:

$$\frac{\delta\nu(\varepsilon)}{\nu_0} \sim -\left(\frac{e^2}{d}\right)\left(\frac{\lambda^2}{d^2}\right)\frac{1}{E_{th}} \times \\ \times \left(\mathrm{arctg}\frac{\varepsilon + A_i}{\gamma} - \mathrm{arctg}\frac{\varepsilon - W_i}{\gamma}\right)\left(\frac{d_i}{l} - \sqrt{\frac{\varepsilon}{E_{th}}}\right),$$

where $E_{\mathrm{th}} = \hbar D/d^2$ – Thouless energy, A_i, W_i – energy boundaries of i-th cluster. Let's point out that, A_i, W_i depend on the size, shape and enviroment of the i-th cluster. In final expression A_i, W_i, d_i have to be substituted by their averaged values (over all clusters) $\bar{A}, \bar{W}, \bar{d}$.

If $\dfrac{\varepsilon}{\bar{W}(\bar{A})} \leqslant 1$:

$$\frac{\delta\nu(\varepsilon)}{\nu_0} \sim -\left(\frac{e^2}{\bar{d}}\right)\left(\frac{\lambda^2}{\bar{d}^2}\right)\frac{1}{E_{\mathrm{th}}}\left[\left(\mathrm{arctg}\frac{\bar{A}}{\gamma} + \mathrm{arctg}\frac{\bar{W}}{\gamma}\right) \times \\ \times \left(\frac{\bar{d}}{l} - \sqrt{\frac{\varepsilon}{E_{\mathrm{th}}}}\right) + \left(\frac{\gamma}{\bar{W}^2 + \gamma^2} - \frac{\gamma}{\bar{A}^2 + \gamma^2}\right)\left(\frac{\bar{d}}{l}\varepsilon\right)\right].$$

For $\varepsilon/\gamma \ll 1$ the square root law dominates in DOS-dependence on electron energy.

From STM/STS-expereiments one can obtain the normalized tunneling conductivity $\sigma_T(eV)$ averaged over all clusters. In the case of non-destructive measurements (modification of initial spectrum caused by tunneling current and non-equilibrium effects are neglected):

$$\left.\frac{\delta\nu(\varepsilon)}{\nu_0}\right|_{\varepsilon = eV} \sim \frac{\delta\sigma(eV)}{\sigma_T(eV)}.$$

For energies higher than 0.1 eV the linear dependence of tunneling conductivity on applied bias voltage can be observed. For cluster size about 10 nm elastic scattering rate can be of order 0.1 eV. Thus the behavior of

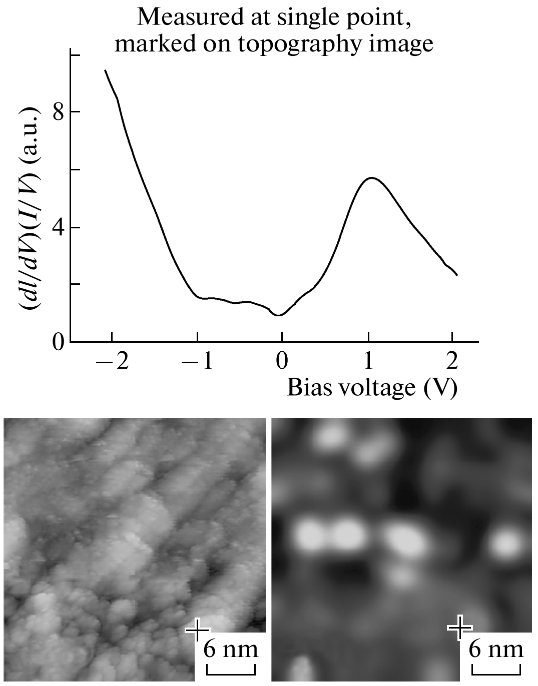

Fig. 3. Constant current STM image (400 × 400 points; $30\times30\,\mathrm{nm}^2$; $V = -2.0\,V$;I=130 pA) and CITS (30×30 nm; $V = 1.09$ V) are shown in the lower left and right parts of Figure correspondingly. LDOS of $Ni_{63.5}Nb_{36.5}$ surface, obtained at single point, marked by the cross, is shown in the upper part of Figure

$\sigma_T(eV)$ averaged over a large number of clusters can be approximated by linear dependence for $eV > 0.1$. Figure 2 demonstrates dependence of normalized tunneling

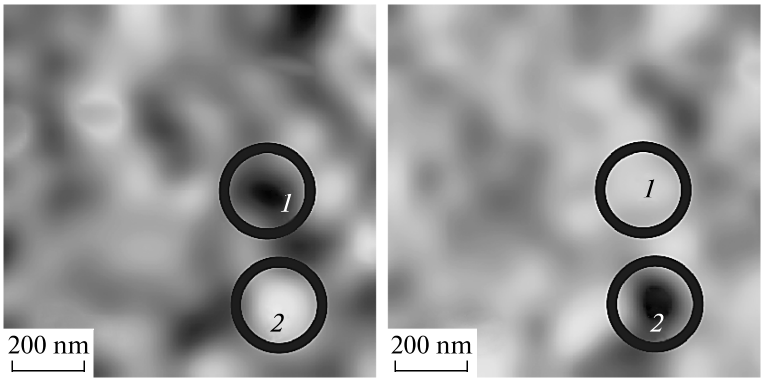

Fig. 4. CITS images ($100 \times 100\,\mathrm{nm}^2$), measured at 0.31 V (left) and -0.28 V (right) show the same site of the surface; *1* and *2* denote two different clusters visible in CITS-mode

conductivity experimental averaged curve on bias voltage. The energy pseudogap can be observed at E_F. The insert in Fig. 2 shows the derivative of depicted curve. This way our experimental data show the opportunity of linear approximation of normalized tunneling conductivity according to theory. The additional features on the averaged normalized tunneling conductivity marked by arrows we associate with the presence of localized states in each different individual cluster on the $Ni_{63.5}Nb_{36.5}$ surface. Each cluster has its own electron structure (Fig. 3) and peaks visible in their LDOS-correspond to energy spectrum of individual cluster localized states. The tunneling spectrum depicted in Fig. 2 demonstrates information about averaged over a great number of surface clusters normalized tunneling conductivity spectra. Let's consider the cluster visible in CITS image and marked by the crosse (Fig. 3) more carefully. In the present case the considered cluster appears in CITS-images as a bright spot. The bright spot in CITS-images corresponds to maxima of tunneling current. Some peaks observed in averaged tunneling conductivity spectrum can be found in individual clusters spectra. We suggest that additional peaks are caused by localized impurity states inside the chosen cluster. As the cluster appears as a bright spot in CITS for both polarities of applied bias voltage we suppose that current image tunneling spectroscopy reflects the specific features of topographic structure which prevaile on peculiarities connected with LDOS. Fig. 4 shows two CITS-images of the same site of the surface. Two different clusters on STM-image are marked by the numbers *1* and *2*. The left image in Fig. 4 is CITS image at positive bias voltage. The upper cluster *1* looks as dark spot while the cluster *2* looks as bright spot. The right image in Fig. 4 is CITS-image at negative bias voltage. In this case we can observe the opposite situation. The upper cluster *1* becomes visible as bright spot while the lower cluster *2* is visible as dark spot. The schematic diagram in Fig. 5 helps to explain the observed behaviour

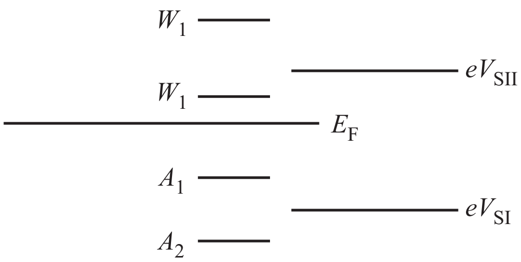

Fig. 5. Schematic diagram of energy levels for two different clusters on $Ni_{63.5}Nb_{36.5}$ surface

of two clusters with different spectrum edges. For cluster *2* most of the states are filled, for cluster *1* – empty. Tunneling current is determined by the local density of states with energies ε: ($E_F < \varepsilon < E_F + eV$):

$$I(eV, r) \sim \int_{E_F}^{E_F+eV} \nu(r, \varepsilon) d\varepsilon.$$

So, for applied bias eV_{SI} cluster *2* appears in CITS-image as a bright spot, while cluster *1* looks like a dark spot. For eV_{SII} the situation is opposite.

Analyzing CITS-images we can obtain some information about the relative values of the energy spectrum boundaries and LDOS of individual clusters.

In conclusion we have have carried out the UHV STM/STS-measurements of bulk metallic glasses surface topography and electronic properties at room temperature. The great number of clusters with size about 5–10 nm have been observed on $Ni_{63.5}Nb_{36.5}$ metallic glass surface. The pseudogap at Fermi energy and linear part of normalized tunneling conductivity spectra dependence on applied bias voltage have been revealed in consistence with suggested theoretical model. The additional features on the averaged normalized tunneling conductivity are connected with the presence of localized states in individual clusters on the $Ni_{63.5}Nb_{36.5}$ surface. The theoretical analysis of electron elastic scattering on the impurities inside each cluster and on the random deffects on the cluster boundaries in the presence of intra-cluster Coulomb interaction of scattering electrons can be applied to explain the experimental results, if the finite values of electron spectrum edges is taken into account.

This work was partially supported by RFBR grants.

1. W. Klement, R. H. Willens, and P. Duwez, Nature **187**, 869 (1960).
2. A. Inoue, Acta mater. **48**, 279 (2000).
3. W. L. Johnson, MRS Bull. **24**, 42 (1999).
4. J. Li, Z. L. Wang, and T. C. Hufnagel, Phys Rev B **65**, 144201 (2002).
5. S. Ashtekar, G. Scott, J. Lyding, and M. Gruebele, J. Phys. Chem. Lett. **1**, 1941 (2010).
6. G. Binnig, H. Rohrer, Ch. Gerber, and E. Weibel, Appl. Phys. Lett. **40**, 178, (1982).
7. G. Binnig, H. Rohrer, Ch. Gerber, and E. Weibel, Phys. Rev. Lett. **49**, 57 (1982).
8. D. V. Louzguine-Luzgin and A. Inoue, J. Nanosci. Nanotech. **5**, 999 (2005).
9. E. Rotenberg, W. Theis, K. Horn, and P. Gille, Nature **406**, 602 (2000).
10. G. F. Syrykh, M. N. Khlopkin, M. G. Zemlyanov et al., Appl. Phys. A **74** [Suppl.] (2002).
11. L. Xia, W. H. Li, S. S. Fang et al., J. Appl. Phys. **99**, 026103 (2006).
12. D. V. Louzguine and A. Inoue, J. Non-Cryst. Solids **337**, 161 (2004).
13. I. Beloborodov, A. Lopatin, V. Vinokur et. al., Rev. Mod. Phys. **79**, 470 (2007).
14. M. Feigel'man and A. Ioselevich, JETP Lett. **81**, 227 (2005).
15. M. Feigel'man, A. Ioselevich, and M. Skvortsov, Phys. Rev. Lett. **93**, 136403, (2004).
16. A. Finkelstein, *Electron Liquid in Disordered Conductors*, Soviet Scientific Reviews, Harwood, London, **14** (1990).
17. B. Altshuler and A. Aronov, *Electron-Electron Interaction in Disordered Conductors*, North-Holland, Amsterdam **10**, 1 (1985).
18. B. Altshuler, A. Aronov, and D. Khmel'nitskii, J. Phys. C **15**, 7367 (1982).
19. B. Altshuler, D. Khmel'nitskii, A. Larkin et al., Phys. Rev. B **22**, 5142, (1980).